Results from a combined test of an electromagnetic liquid argon calorimeter with a hadronic scintillating-tile calorimeter

Ziad Ajaltouni, V. Tisserand, S. Jezequel, F. Albiol, A. Alifanov, P. Amaral, G. Ambrosini, A. Amorim, K J. Anderson, A. Astvatsaturov, et al.

EUROPEAN ORGANIZATION FOR NUCLEAR RESEARCH

CERN-PPE/96-178
8 November 1996

RESULTS FROM A COMBINED TEST OF AN ELECTROMAGNETIC LIQUID ARGON CALORIMETER WITH A HADRONIC SCINTILLATING-TILE CALORIMETER

ATLAS Collaboration
(Calorimetry and Data Acquisition)

Z. Ajaltouni[10], F. Albiol[33], A. Alifanov[19], P. Amaral[14], G. Ambrosini[23, 1)], A. Amorim[14], K. Anderson[9], A. Astvatsaturov[12], B. Aubert[2], E. Augé[21], D. Autiero[24], G. Azuelos[20], F. Badaud[10], L. Baisin[8], G. Battistoni[18], A. Bazan[2], C. Bee[8, 2)], G. Bellettini[24], S. Berglund[30], J.C. Berset[8], C. Blaj[7], G. Blanchot[5], E. Blucher[9], A. Bogush[19], C. Bohm[30], V. Boldea[7], O. Borisov[12], M. Bosman[5], N. Bouhemaid[10], P. Brette[10], C. Bromberg[17], M. Brossard[10], J. Budagov[12], S. Buono[8], L. Caloba[28], D.V. Camin[18], B. Canton[22], P. Casado[5], D. Cavalli[18], M. Cavalli-Sforza[5], V. Cavasinni[24], R. Chadelas[10], R. Chase[21], A. Chekhtman[16], J.-C. Chevaleyre[10], J.L. Chevalley[8], I. Chirikov-Zorin[12], G. Chlachidze[12], J.C. Chollet[21], M. Cobal[8], F. Cogswell[32], J. Colas[2], J. Collot[13], S. Cologna[24], S. Constantinescu[7], G. Costa[18], D. Costanzo[24], L. Cozzi[18], M. Crouau[10], P. Dargent[16], F. Daudon[10], M. David[14], T. Davidek[25], J. Dawson[3], K. De[4], C. de la Taille[21], T. Del Prete[24], P. Depommier[20], P. de Saintignon[13], A. De Santo[24], B. Dinkespiller[16], B. Di Girolamo[24], S. Dita[7], J. Dolejsi[25], Z. Dolezal[25], R. Downing[32], J.-J. Dugne[10], P.-Y. Duval[16], D. Dzahini[13], I. Efthymiopoulos[5, 3)], D. Errede[32], S. Errede[32], F. Etienne[16], H. Evans[9], P. Fassnacht[16], N. Fedyakin[18], A. Ferrari[18], P. Ferreira[14], A. Ferrer[33], V. Flaminio[24], D. Fouchez[16], D. Fournier[21], G. Fumagalli[23], E. Gallas[4], M. Gaspar[28], F. Gianotti[8, 4)], O. Gildemeister[8], D.M. Gingrich[1], V. Glagolev[12], V. Golubev[19], A. Gomes[14], J. Gonzalez[21] H.A. Gordon[6], V. Grabsky[35], H. Hakopian[35], M. Haney[32], S. Hellman[30], A. Henriques[8], S. Holmgren[30], P.F. Honoré[33], J.Y. Hostachy[13], J. Huston[17], Yu. Ivanyushenkov[5], S. Jezequel[2], E. Johansson[30], K. Jon-And[30], R. Jones[8], A. Juste[5], S. Kakurin[12], G. Karapetian[8], A. Karyukhin[27], Yu. Khokhlov[27], V. Klyukhin[27], V. Kolomoets[12], S. Kopikov[27], M. Kostrikov[27], V. Kovtun[12], V. Kukhtin[12], M. Kulagin[27], Y. Kulchitsky[19, 5)], G. Laborie[13], S. Lami[24], V. Lapin[27], A. Lebedev[12], M. Lefebvre[34] T. Leflour[2], R. Leitner[25], E. León-Florián[20], C. Leroy[20], A. Le Van Suu[16], J. Li[4], I. Liba[12], O. Linossier[2], M. Lokajicek[26], Yu. Lomakin[12], O. Lomakina[12], B. Lund-Jensen[31] G. Mahout[13], A. Maio[14], S. Malyukov[12], L. Mandelli[18], B. Mansoulié[29], L. Mapelli[8], C.P. Marin[8], F. Marroquin[28], L. Martin[16], M. Mazzanti[18], E. Mazzoni[24], F. Merritt[9], B. Michel[10], R. Miller[17], I. Minashvili[12], A. Miotto[16], L. Miralles[5], E. Mnatsakanian[35], E. Monnier[16], G. Montarou[10], G. Mornacchi[8], G.S. Muanza[10], E. Nagy[16], S. Nemecek[26], M. Nessi[8], S. Nicoleau[2], J.M. Noppe[21], C. Olivetto[16], S. Orteu[5], C. Padilla[5], D. Pallin[10], D. Pantea[12 6)], G. Parrour[21], A. Pereira[28], L. Perini[18], J.A. Perlas[5], P. Pétroff[21], J. Pilcher[9], J.L. Pinfold[1] L. Poggioli[8], S. Poirot[10], G. Polesello[23], L. Price[3], Y. Protopopov[27], J. Proudfoot[3], O. Pukhov[12], V. Radeka[6], D. Rahm[6], G. Reinmuth[10], J.F. Renardy[29], G. Renzoni[24], S. Resconi[18], R. Richards[17], I. Riu[5], V. Romanov[12], B. Ronceux[5], V. Rumyantsev[19, 5)], N. Russakovich[12], P. Sala[18], H. Sanders[9], G. Sauvage[2], P. Savard[20], A. Savoy-Navarro[22] L. Sawyer[4],

[1)] Now at University of Bern, Switzerland
[2)] Now at University of Zurich, Switzerland
[3)] Now at CERN, Switzerland
[4)] Also University of Milano, Italy
[5)] Also JINR Dubna, Russia
[6)] Now at Institute for Atomic Physics, Bucharest, Romania

L.-P. Says[10], A. Schaffer[21], C. Scheel[15], P. Schwemling[22], J. Schwindling[29], N. Seguin-Moreau[21], J.M. Seixas[28], B. Sellden[30], M. Seman[11], A. Semenov[12], V. Senchishin[12], L. Serin[21], A. Shchelchkov[12], V. Shevtsov[12], M. Shochet[9], V. Sidorov[27], V. Simaitis[32], S. Simion[29], A. Sissakian[12], A. Solodkov[10], P. Sonderegger[8], K. Soustruznik[25], R. Stanek[3], E. Starchenko[27], D. Stephani[6], R. Stephens[4], S. Studenov[12], M. Suk[25], A. Surkov[27], F. Tang[9], S. Tardell[30], P. Tas[25], J. Teiger[29], F. Teubert[5], J. Thaler[32], V. Tisserand[21], S. Tisserant[16], S. Tokar[12], N. Topilin[12], Z. Trka[25], A. Turcot[9], M. Turcotte[4], S. Valkar[25], A. Vartapetian[35], F. Vazeille[10], I. Vichou[21, 7)], V. Vinogradov[12], S. Vorozhtsov[12], V. Vuillemin[8], D. Wagner[9], A. White[4], I. Wingerter-Seez[2], N. Yamdagni[30], G. Yarygin[12], C. Yosef[17], A. Zaitsev[27], M. Zdrazil[25], R. Zitoun[2], Y.P. Zolnierowski[2]

[1] University of Alberta, Edmonton, Alberta, Canada
[2] LAPP, Annecy, France
[3] Argonne National Laboratory, USA
[4] University of Texas at Arlington, USA
[5] Institut de Fisica d'Altes Energies, Universitat Autònoma de Barcelona, Spain
[6] Brookhaven National Laboratory, Upton, USA
[7] Institute of Atomic Physics, Bucharest, Rumania
[8] CERN, Geneva, Switzerland
[9] University of Chicago, USA
[10] LPC Clermont–Ferrand, Université Blaise Pascal / CNRS–IN2P3, France
[11] Nevis Laboratories, Columbia University, Irvington NY, USA
[12] JINR Dubna, Russia
[13] ISN, Université Joseph Fourier /CNRS-IN2P3, Grenoble, France
[14] LIP-Lisbon and FCUL-Univ. of Lisbon
[15] Univ. Autonoma Madrid, Spain
[16] CPP Marseille, France
[17] Michigan State University, USA
[18] Milano University and INFN, Milano, Italy
[19] Institute of Physics ASB, Minsk, Belarus
[20] University of Montreal, Canada
[21] LAL, Orsay, France
[22] LPNHE, Universites de Paris VI et VII, France
[23] Pavia University and INFN, Pavia, Italy
[24] Pisa University and INFN, Pisa, Italy
[25] Charles University, Prague, Czech Republic
[26] Academy of Science, Prague, Czech Republic
[27] Institute for High Energy Physics, Protvino, Russia
[28] COPPE/EE/UFRJ, Rio de Janeiro, Brazil
[29] CEA, DSM/DAPNIA/SPP, CE Saclay, Gif-sur-Yvette, France
[30] Stockohlm University, Sweden
[31] Royal Institute of Technology, Stockholm, Sweden
[32] University of Illinois, USA
[33] IFIC Valencia, Spain
[34] University of Victoria, British Columbia, Canada
[35] Yerevan Physics Institute, Armenia

Accepted by Nucl. Instr. Meth.

[7)] Now at Universitat Autònoma de Barcelona, Spain

Abstract

The first combined test of an electromagnetic liquid argon accordion calorimeter and a hadronic scintillating-tile calorimeter was carried out at the CERN SPS. These devices are prototypes of the barrel calorimeter of the future ATLAS experiment at the LHC. The energy resolution of pions in the energy range from 20 to 300 GeV at an incident angle θ of about 11° is well-described by the expression $\sigma/E = ((46.5 \pm 6.0)\%/\sqrt{E} + (1.2 \pm 0.3)\%) \oplus (3.2 \pm 0.4)$ GeV$/E$. Shower profiles, shower leakage, and the angular resolution of hadronic showers were also studied.

1 INTRODUCTION

The future ATLAS experiment [1] at the CERN Large Hadron Collider (LHC) will include in the central ('barrel') region a calorimeter system composed of two separate units: a liquid argon (LAr) electromagnetic (EM) calorimeter with hermetic accordion geometry, and a scintillating-tile hadronic calorimeter using iron as the absorber, in which the tiles are placed perpendicular to the colliding beams. This system must be capable of identifying electrons, photons, and jets and of reconstructing their energies and angles in the difficult LHC environment, as well as of measuring missing transverse energy in the event. The barrel calorimeter will cover the ATLAS central region in a pseudorapidity[1)] range of $|\eta| \leq 1.4$.

In this paper the results of the first test of the electromagnetic and hadronic calorimeter prototypes in a combined setup are presented. The paper is organized as follows: in Section 2 the two calorimeter prototypes are briefly described, and in Section 3 the combined test beam setup and the data selection procedure are presented. The results are discussed in Section 4, with special emphasis on the energy resolution of hadronic showers. Finally Section 5 contains a summary and the conclusions.

2 THE CALORIMETER PROTOTYPES

Over the past few years, several prototypes of the two calorimeters went through a series of separate test [2],[3]. In 1994, for the first time, the calorimeters were tested in a combined mode. An azimuthal sector of the ATLAS barrel calorimeter was reproduced by placing the hadronic device downstream of the EM calorimeter.

2.1 The electromagnetic liquid argon calorimeter

The electromagnetic LAr calorimeter prototype consists of a stack of three azimuthal modules, each one spanning 9° in azimuth and extending over 2 m along the *z* direction. The calorimeter structure is defined by 2.2 mm thick steel-plated lead absorbers, folded to an accordion shape and separated by 3.8 mm gaps, filled with liquid argon; the signals are collected by Kapton electrodes located in the gaps. The calorimeter extends from an inner radius of 131.5 cm to an outer radius of 182.6 cm, representing (at η = 0) a total of 25 radiation lengths (X_0), or 1.22 interaction lengths (λ) for protons. The calorimeter is longitudinally segmented into three compartments of $9\ X_0$, $9\ X_0$ and $7\ X_0$, respectively. The $\eta \times \phi$ segmentation is 0.018×0.02 for the first two longitudinal compartments and 0.036×0.02 for the last compartment. Each read-out cell has full projective geometry in η and in ϕ.

The calorimeter was located inside a large cylindrical cryostat with 2 m internal diameter, filled with liquid argon. The cryostat is made out of a 8 mm thick inner stainless-steel vessel, isolated by 30 cm of low-density foam (Rohacell), itself protected by a 1.2 mm thick aluminum outer wall. The read-out electrodes are equipped with different types of preamplifiers, hybrid charge-sensitive preamplifiers based on Si JFETs and monolithic GaAs MESFETs, working at LAr temperature, and warm current preamplifiers. Each preamplifier is followed by a shaping amplifier (with a peaking time $t_p(\delta) \simeq 20$ ns), a Track&Hold circuit and a 12-bit ADC. To correct for the different channel gains a 'voltage driven' calibration is used. The signal-to-energy conversion factor is obtained using electron beams of different energies. More details about this prototype can be found in Refs. [1, 2].

[1)] In the collider reference system, which has been adopted here, the *z* axis indicates the LHC beam line, the *x* and *y* axis the horizontal and the vertical direction, while ϕ and θ are the azimuthal and polar angle, respectively. The pseudorapidity is defined as $\eta = -\ln(\tan(\theta/2))$.

For the analysis described in this paper only part of the calorimeter was used, namely a matrix of 11×11 cells centred around the nominal beam spot for the first two longitudinal compartments and of 5×11 cells for the third. This corresponds to a front face of about $25 \times 25\,\mathrm{cm}^2$.

A $3\,X_0$ thick preconverter ('preshower') device with fine η and ϕ segmentation was placed in the cryostat directly in front of the accordion calorimeter; signals from this device were used in the analysis to reject events with more than one track entering the LAr calorimeter.

2.2 The hadronic Tile calorimeter

The hadron calorimeter is a sampling device using steel as the absorber and scintillating tiles as the active material. The innovative feature of the design is the orientation of the tiles which are placed in planes perpendicular to the *z* direction; for a better sampling homogeneity the 3 mm thick scintillators are staggered in the radial direction. The tiles are separated along *z* by 14 mm of steel, giving a steel/scintillator volume ratio of 4.7. Wavelength shifting fibres (WLS) running radially collect light from the tiles at both of their open edges.

The hadron calorimeter prototype consists of an azimuthal stack of five modules. Each module covers $2\pi/64$ in azimuth and extends 1 m along the *z* direction, such that the front face covers 100×20 cm^2. The radial depth, from an inner radius of 200 cm to an outer radius of 380 cm, accounts for 8.9 λ at η = 0 (80.5 X_0). Read-out cells are defined by grouping together a bundle of fibres into one photomultiplier (PMT). Each of the 100 cells is read out by two PMTs and is fully projective in azimuth (with $\Delta\phi = 2\pi/64 \approx 0.1$), while the segmentation along the *z* axis is made by grouping fibres into read-out cells spanning $\Delta z = 20$ cm ($\Delta\eta \approx 0.1$) and is therefore not projective. Each module is read out in four longitudinal segments (corresponding to about 1.5, 2, 2.5 and 3 λ at η = 0).

The gain of the PMTs was set to deliver $\simeq$ 6 pC/GeV for incident electrons. The high voltage of each PMT was adjusted such that an equal response is obtained within a few per cent by running a radioactive source through each scintillating tile. This procedure gives a first-pass cell intercalibration because the current induced in each PMT is proportional to its gain and to the photoelectron yield of the read-out cell. This intercalibration was further refined offline. A pulsed laser system which illuminates each PMT by means of clear fibres was used to monitor short-term gain drifts. The PMT signal was digitized by a 12-bit charge-sensitive ADC which, in addition to a direct digital output, provided a second digital output with an internal amplification of 7.5, thereby giving an effective dynamic range of 15 bits.

More details of this prototype can be found in Refs. [1, 3, 4, 5].

3 EXPERIMENTAL SETUP AND TEST BEAM DATA

To simulate the ATLAS setup the Tile calorimeter prototype was placed downstream of the LAr cryostat as shown in Fig. 1.

To optimize the containment of hadronic showers the electromagnetic calorimeter was located as close as possible to the back of the cryostat. Early showers in the liquid argon were kept to a minimum by placing light foam material in the cryostat upstream of the calorimeter.

The hadronic calorimeter was placed on a table built for this test, directly behind and as close as possible to the LAr cryostat. Nevertheless the distance between the active parts of the two detectors was ≈ 55 cm, a factor of two larger than in the ATLAS design configuration. The material between the two calorimeters was about $1.7\ X_0$, which is close to the ATLAS design value; however, the test cryostat is mostly steel, with a higher Z than that of the ATLAS cryostat which will be built out of aluminium.

The requirements of shower containment and space constraints meant that the two calorimeters be placed with their central axes at an angle to the beam of 11.3°. At this angle the EM calorimeter no longer pointed exactly to the nominal interaction point; however, cell projectivity along the azimuthal direction was maintained. At 11.3° the two calorimeters have an active thickness of 10.3 λ (10.1 λ at η = 0, to be compared with 9.6 λ at η = 0 for the ATLAS detector).

To detect punchthrough particles and to measure the effect of longitudinal leakage a 'muon wall' consisting of 10 scintillator counters (each 2 cm thick) was located behind the calorimeters at a distance of about 1 metre. The counters formed an array covering approximately 73 cm in the vertical and 96 cm in the horizontal direction. The muon wall counters were separated from the last Tile calorimeter compartment by 0.7 λ of structural materials.

All data were taken on the H8 beam of the CERN SPS, with pion and electron beams of 20, 50, 100, 150, 200 and 300 GeV/*c*. The electron data were used to obtain the signal-to-energy conversion factor for the EM calorimeter. Beam quality and geometry were monitored with a set of beam chambers and trigger hodoscopes placed upstream of the LAr cryostat. The momentum bite of the beam was always less than 0.5%. Single-track pion events were selected offline by requiring the pulse height of the beam scintillation counters and the energy released in the preshower of the electromagnetic calorimeter to be compatible with that of a single particle. Beam halo events were removed with appropriate cuts on the horizontal and vertical positions of the incoming track impact point as measured with the two beam chambers.

A detailed study was performed to determine the noise level in the combined setup. To measure the noise level independently in the two calorimeters, pedestal triggers were recorded before and after the SPS beam burst with the same rate as the particle triggers. The total noise in the read-out system is the quadratic sum of an incoherent random component (σ_{incoh}) from the electronics, and a coherent part (σ_{coh}), which may arise from various sources, like cross-talk or pick-up from external sources. The incoherent noise scales with $\sqrt{N_{ch}}$, where N_{ch} is the number of read-out cells used to reconstruct the energy, while the coherent noise is proportional to N_{ch}. Thus even small coherent noise levels may degrade the resolution significantly when relatively large numbers of read-out cells are involved as is the case here. From the pedestal trigger data the total noise for the two calorimeters was estimated to be about 1.5 GeV, of which 0.9 GeV comes from coherent noise.

4 PION BEAM RESULTS

The main purpose of the test described in this paper was to demonstrate that the proposed combination of two calorimeters allows one to reconstruct the energy of incident hadrons with resolution and linearity within the goals of the ATLAS experiment[1]. Therefore the analysis presented in this section is focused on these aspects of the combined calorimeter performance. However, the data were also studied to extract information on the longitudinal energy deposition profiles, the angular resolution for hadrons, and the hadronic shower leakage.

It is well known that the energy resolution of sampling calorimeters for hadrons is affected by several factors, among which the sampling fluctuations, the non-compensating nature of the calorimeter, and the electronic noise (at low energy) play an important role. For this combined setup, two further factors contribute to the resolution and must be taken into account in reconstructing the incident hadron energy:

1. The energy losses in the passive material between the LAr and Tile calorimeters, mostly due to the outer cryostat wall. These can be important when the hadron interacts in the EM compartment (about 56% of cases),
2. The difference between the responses of the EM and Tile calorimeters to the electromag-

netic and hadronic components of the hadron shower, i.e. the different non-compensation of the two calorimeters.

To reconstruct the hadron energy, two different algorithms were developed [6]. The first method, referred to in the following as the 'benchmark approach', is designed to be simple. With this method the incident energy is reconstructed with a minimal number of parameters (all energy independent with the exception of one). The second method, the 'weighting technique' is based on a separate correction parameter for each longitudinal compartment of the two calorimeters. These parameters are independently optimized for each incident energy and are indeed found to be energy-dependent. In using these algorithms no noise cuts were applied to the data.

4.1 Energy reconstruction using a 'benchmark' approach

In the 'benchmark' algorithm, a two step procedure is adopted to reconstruct the nominal beam energy: first, the energy of the particle is obtained as the sum of several terms, and the intervening parameters are optimized by minimizing the fractional energy resolution σ/E_0. This first-pass energy E_0 is rescaled to the nominal beam energy in a second step.

In the first step, the incident hadron energy is written as the sum of four terms:

1. The sum of the signals in the electromagnetic calorimeter, E_{em}, expressed in GeV using the calibration from electrons.
2. A term proportional to the charge deposited in the hadronic calorimeter, Q_{had}.
3. A term to account for the energy lost in the cryostat, E_{cryo}. This term is taken to be proportional to the geometric mean of the energy released in the last electromagnetic compartment (E_{em_3}) and the first hadronic compartment (Q_{had_1}). Monte Carlo studies showed agreement with this $ansatz$.
4. A negative correction term, proportional to E_{em}^2. For showers that begin in the EM calorimeter, this term crudely accounts for its non-compensating behaviour.

The first-pass energy E_0 is then

$$E_0 = E_{em} + a \cdot Q_{had} + b \cdot \sqrt{|E_{em_3} \cdot a \cdot Q_{had_1}|} + c \cdot E_{em}^2; \qquad (1)$$

the parameters a, b and c were determined by minimizing the fractional energy resolution of 300 GeV pions. The values of the three parameters are $a = 0.172$ GeV/pC, b = 0.44 and c = $-$ 0.00038 GeV^{-1}.

To clarify and further justify the procedure, in Fig. 2 the values of E_0 for different values of E_{em} are shown for the 300 GeV pion data. Also shown are the results of adding only the first two or the first three terms of E_0. Adding the cryostat correction term E_{cryo} makes the sum $E_{em} + a \cdot Q_{had} + b \cdot E_{cryo}$ independent of the energy in the EM calorimeter for $E_{em} \leq 100$ GeV. This correction is independent of the incident pion energy: the distributions of the energy loss in the cryostat (using the above $ansatz$) as a function of the energy fraction f_{em} deposited in the electromagnetic compartment are similar for different beam energies and peak at $f_{em} \simeq 0.2$. Figure 2 also shows that adding the term $c \cdot E_{em}^2$ makes the reconstructed energy independent of the energy deposited in the electromagnetic compartment. This procedure minimizes the fractional energy resolution, however the reconstructed energy is systematically underestimated, due to the fact that both calorimeters are non-compensating (e/$\pi > 1$, see Ref. [3]); for this reason an additional step of rescaling is necessary.

In this second step the mean and σ values of the first-pass energy distributions are extracted with Gaussian fits over a $\pm 2\sigma$ range. The difference between the nominal beam energy (E_{beam}) and the mean E_0 values is shown in Fig. 3 (black dots) as a function of E_{beam}. To rescale the first pass energy E_0 to the beam energy E_{beam} the approach of Refs. [7, 8] was taken. In a

non-compensating calorimeter, the mean visible energy is given by [7].

$$E_{beam}\left[1-(1-F_{\pi^\circ})\left(1-\frac{\epsilon_h}{\epsilon_e}\right)\right] \tag{2}$$

where ϵ_h and ϵ_e are the calorimeter response to hadrons and electrons, and F_{π° is the energy-dependent fraction of the incident hadron energy which is transferred to the electromagnetic sector. In this paper, the mean visible energy is identified with E_0, and the values of $(\frac{\epsilon_h}{\epsilon_e})_{em}$ and $(\frac{\epsilon_h}{\epsilon_e})_{had}$ (different for the two calorimeters) were found by fitting for all beam energies the expression

$$E_{beam}=\frac{E_0}{f_{em}\left[1-F_h\left(1-\left(\frac{\epsilon_h}{\epsilon_e}\right)_{em}\right)\right]+(1-f_{em})\left[1-F_h\left(1-\left(\frac{\epsilon_h}{\epsilon_e}\right)_{had}\right)\right]} \tag{3}$$

where $F_h \equiv 1-F_{\pi^\circ}$, F_{π° is given as a function of beam energy as in Ref. [8] and two terms in the denominator are weighted by the average fractions of energy deposited in the accordion (f_{em}) and Tile calorimeters, taken from the data. The fit gives $(\frac{\epsilon_h}{\epsilon_e})_{em} = 0.53 \pm 0.01$ and $(\frac{\epsilon_h}{\epsilon_e})_{had} = 0.82 \pm 0.01$. These values do not have the usual meaning because they are determined not from the raw signals but from E_0, which already includes corrections. In particular, the quadratic correction of the EM energy in eq. 1 pushes down the value of $\frac{\epsilon_h}{\epsilon_e}$ for the EM calorimeter.

To calculate the distribution of reconstructed energies E_{rec} eq. 3 is used, replacing E_{beam} with E_{rec} and introducing the approximations $F_{\pi^\circ}(E_{beam}) = F_{\pi^\circ}(E_0)$ and $f_{em}(E_{beam}) = f_{em}(E_0)$.

The rescaled mean values E_{rec}, the resolutions σ_{rec} and the fractional resolutions σ_{rec}/E_{rec} are given in Table 1 for the various beam energies. The rescaling factors vary between 1.25 and 1.12 with the beam energy. The reconstructed energy spectra are shown in Fig. 4 for the six energies at which data were taken. The results of the Gaussian fits are also shown in the same figure.

The energy distributions of Fig. 4 show low energy tails, that at high energies are mostly due to events which suffer from an incomplete longitudinal shower containment. These low energy tails can be reduced by removing the events with a signal in the muon wall [9] behind the calorimeter, as shown as an example in Fig. 5 for the 300 GeV pions. This implies that there is some longitudinal leakage even after a calorimeter about 10 λ thick. Further punchthrough studies are given in Section 4.5.

To determine the e/π ratio for the combined setup the pion energy was reconstructed with the expression

$$E^{\pi}_{rec} = E^{\pi}_{em} + a\cdot Q^{\pi}_{had} + b\cdot\sqrt{|E^{\pi}_{em_3}\cdot a\cdot Q^{\pi}_{had_1}|}, \tag{4}$$

where a and b have the values given above. The cryostat term must be added in order to avoid a systematic underestimate of the response to pions. The electron response is directly available from the test beam data. The resulting e/π ratios as a function of the pion beam energy are given in Fig. 6; they lie between 1.24 and 1.12. The response to pions relative to electrons is seen to increase with energy as expected, because the fraction of electromagnetic energy in an hadronic shower increases with energy [10, 7, 8]. The e/π values obtained with a standalone FLUKA simulation (see discussion in Section 4.3) are in good agreement with the experimental ones, as shown in the plot.

4.2 Energy reconstruction using a sampling correction technique

The second approach to reconstruct the pion energy relies on the experience from previous calorimeter studies [3, 11], which suggests that correcting the energy in each longitudinal compartment ('sampling') may improve both the energy resolution and the linearity. The

correction strategy chosen here is to adjust downwards the response of the read-out cells with a large signal to compensate for the response to large EM energy clusters, typically due to π^0 production.

A separate weighting parameter was introduced for each longitudinal sampling. The energy measured in each read–out cell E_i is corrected according to the formula:

$$E_i^{corr} = E_i \cdot (1 - W_j \frac{E_i}{E_j}), \tag{5}$$

where E_j is the energy sum over all cells of sampling j and W_j is the (positive) weight to be optimized for each sampling j. In total eight energy-dependent parameters must be determined: one for each of the seven samplings, plus an additional conversion factor f to convert the hadronic signal from charge to energy.

The two-step procedure described above was adopted to reconstruct the nominal beam energy: first, the measured energy in the two calorimeters, E_0^{corr}, was reconstructed by minimizing the energy resolution, σ_0/E_0^{corr}; E_0^{corr} was then rescaled to the nominal beam energy. This second step is needed because of the negative sign of the correction.

The eight parameters were determined at each beam energy with the following iterative method:

1. The weights for the four longitudinal samplings of the Tile calorimeter were determined first. Events with no nuclear interaction in the electromagnetic calorimeter were selected. Using those events the weight of the last sampling was optimized by setting to zero the weight of all the other hadronic samplings upstream and by minimizing σ_0/E_0^{corr} in the Tile calorimeter. The procedure was repeated for the third, second and first sampling, allowing at each iteration a weight different from zero in that sampling but not in the hadronic ones upstream. In each of the four iterations the weights of all samplings being corrected in that iteration were reoptimized starting from the value obtained in the previous step.
2. The signal obtained summing all the corrected signals E_i^{corr} from the hadron calorimeter was normalized to the beam energy multiplying it by a charge-to-energy conversion factor f.
3. The energy lost in the cryostat, parametrized as in the benchmark approach and with the same weight $b = 0.44$ was added.
4. Finally the weights for the three samplings of the EM calorimeter were determined with another iterative procedure, starting by allowing nuclear interactions in the third (last) sampling and reoptimizing the weights of all samplings downstream of the one being considered as well as the conversion factor f at each of the three steps.

The energy dependence of the eight parameters as a function of the beam energy is shown in Fig. 7(a)-7(d) for the four hadronic samplings, in Fig. 7(e)-7(g) for the three electromagnetic samplings, and in Fig. 7(h) for the conversion factor f. The weights relative to the fourth hadronic sampling are null at all the energies. This is because it has been required for the weights to be positive, which means that they reduce the energy reconstructed in the sampling. However, in this case the correction should be such as to compensate for the presence of longitudinal leakages by increasing the reconstructed energy. As a result the weights are equal to 0.

All parameters are seen to be a smooth function of the beam energy, and were fitted with linear functions of the latter. The values from these fits were used as the final weights.

The procedure followed for rescaling the mean value of E_0^{corr} to the nominal beam energy is the same already described for the benchmark approach. The difference between the beam energy and the corrected first-pass energy E_0^{corr} is shown in Fig. 3 (empty circles) as a function

of the beam energy. The fit yields a rescaling factor between 1.17 and 1.10, depending on the energy; the two parameters of the fit are $(\frac{e_h}{e_e})_{em} = 0.71 \pm 0.01$ and $(\frac{e_h}{e_e})_{had} = 0.83 \pm 0.01$. As an example, Fig. 8 shows the energy spectrum after applying the weighting and rescaling procedure to the 300 GeV pion data. The reconstructed mean values E_{rec}, the width σ_{rec}, and the energy resolution σ_{rec}/E_{rec} are summarized in Table 2 for all beam energies.

4.3 Resolution and linearity

The energy resolutions (σ/E) obtained with the two energy reconstruction methods are plotted in Fig. 9 as a function of $1/\sqrt{E}$.

The energy resolutions obtained from the weighting technique are fitted with the function:

$$\frac{\sigma}{E} = \left[\frac{(46.5 \pm 6.0)\ \%}{\sqrt{E}} + (1.2 \pm 0.3)\ \%\right] \oplus \frac{(3.2 \pm 0.4)\ \text{GeV}}{E} \qquad (6)$$

where *E* is in GeV, the symbol $\oplus$ indicates a sum in quadrature and the last term has the form expected for the electronic noise. A linear sum of sampling and constant terms has been used for the fit, which is shown in Fig. 9. The weighting approach shows to be effective in reducing both the sampling and the constant term, with respect to the benchmark case (which gives respectively (52.1 ± 5.5) %/$\sqrt{E}$, (1.9 ± 0.3) % and a similar noise term). The weighting approach resolutions have been also fitted with a quadratic sum, which gives a slightly higher sampling and constant terms ((55.4 ± 4.0) %/$\sqrt{E}$ and (2.3 ± 0.3) %, respectively) and a similar noise term.

The combined setup was simulated both with GEANT-CALOR [12, 13] and with the standalone FLUKA [14] program. The former uses the CALOR hadronic package up to 5-10 GeV and an obsolete version of the FLUKA hadronic models above 10 GeV. Its application to the LAr and Tile calorimeters are described in Refs. [2, 3, 5]; a discussion of the hadronic packages implemented into GEANT and comparisons with nuclear interaction experimental data can be found in [15]. The physical models of FLUKA, which have been already successfully used for the analysis of muon radiative interactions in the same experimental setup [16, 17], are described in [14]. The Monte Carlo predictions, using a 'benchmark-like' technique to reconstruct the energy with the addition of the same noise term of 1.5 GeV/*E* (see discussion above), are also shown in Fig. 9. The FLUKA and GEANT results have been calibrated in the electron scale, simulating the response of both calorimeters in standalone mode to monoenergetic electrons. The fitted benchmark parameters are consistent with the experimental ones. A 15% proton contamination has been added to the pion events at 20 GeV, the only point taken with positive beam polarity. The amount of proton contamination has been estimated using a FLUKA simulation of the SPS target, which was checked to be in reasonable agreement with a few available experimental data both at low [18] and high [19] momenta, for similar targets and energies. The effect of the proton contamination in the Monte Carlo data is to raise the fractional resolution, i.e. in FLUKA, from 16.9% to 17.7%.

Above 100 GeV the energy resolution of the combined calorimeter is similar to the one expected from both Monte Carlo simulations, as well as to the resolution obtained in a separate beam test of the Tile calorimeter [3] alone (shown by the $\star$ symbols in Figure 9). At lower energies combined data resolutions are significantly larger than those obtained in the Tile standalone. This shows up in the fits as a "noise" term larger than the one experimentally determined. This increase partially comes from the beam contamination at 20 GeV.

The experimental resolutions are in a reasonable agreement with FLUKA, which has a sampling, a constant and a noise term respectively of (48.2 ± 5.1) %/$\sqrt{E}$, (1.7 ± 0.4) % and

(2.5 ± 0.3) GeV/E, as given by a linear fit. Although the data degrade more rapidly the trend is not much different. The small discrepancy could point to some residual experimental problem, such as non-optimal beam quality, at the lowest energies. An opportunity to clarify this point will come with the data from the next combined calorimeter test run.

The linearity of the calorimeter response to pions is shown in Fig. 10, in which the E_{rec}/E_{beam} ratio is normalized to 1 at 100 GeV. A comparison can be made between the results obtained with the two energy reconstruction methods. With the benchmark algorithm the response to pions is linear within $\pm 1\%$ over the full energy range of the data. The results of the weighting method are similar except for the points at 20 and 300 GeV which are slightly degraded.

It can be concluded that the weighting technique improves the energy resolution but does not improve the linearity obtained with the simplest approach.

4.4 Longitudinal energy deposition profiles and angular resolution

The mean raw energy deposited in each sampling can be plotted against the calorimeter depth to give a useful representation of the longitudinal development of showers. Figure 11 shows the longitudinal profiles for pions of 50 and 300 GeV compared with the Monte Carlo predictions. The GEANT simulation reproduces reasonably well the shape of the data in the hadronic compartment. However, in the electromagnetic part the shower develops later than in the data. Conversely, the FLUKA results are in agreement with the data at both energies and in both calorimeters. Figure 12 shows the percentage of the total raw energy released in the electromagnetic and hadronic calorimeter for different beam energies. In all the cases more than 50% of the energy is released in the hadronic compartment. FLUKA results are in almost perfect agreement with the data, while GEANT-CALOR systematically predicts a lower total energy released in the electromagnetic compartment with respect to the data.

Both this effect and the disagreement in the longitudinal profiles can be attributed to the fact that hadronic cascades are not well simulated [15] by GEANT-CALOR. Studies [20] have been performed which show that the simulation fails to reproduce the non-linear behaviour of the data, due to a difference in the e/h ratio (too small) and in the fraction of π^0 produced.

The data were also used to determine the angular resolution of hadronic showers. The knowledge of the direction of the decay-jets can be useful to improve the mass reconstruction of particles decaying into a pair of jets.

To determine the angular resolution of the polar angle for a hadronic shower the mean position was measured independently in each radial compartment of the electromagnetic and hadronic calorimeter on an event-to-event basis [21]. The polar angle θ was determined for each event by a linear fit to the equation:

$$\overline{z}_j = \tan(\theta) \cdot r_j + b, \tag{7}$$

where $\overline{z}_j$ is the centre of gravity of the energy deposition in a sampling j averaged over all contributing cells in azimuth, r_j is the known radial position of the compartment taken in the centre, and b is an arbitrary intercept. For each energy the angular resolution is obtained from a Gaussian fit to the reconstructed beam angle θ. The angular resolution σ_θ is shown in Fig. 13 as a function of beam energy; it is a linear function of $1/\sqrt{E}$. The fit gives $\sigma_\theta = (243.1 \pm 8.9)/\sqrt{E} + (12.1 \pm 0.7)$ mrad, resulting in an angular resolution of $\sigma_\theta = 1.5^\circ$ for hadron showers from 300 GeV pions. This is about a factor of five better than the Tile calorimeter cell size. Averaging over all energies a mean polar angle $\overline{\theta}$ = (11.23 $\pm$ 0.01)$^\circ$ was obtained which agrees well with the nominal beam angle of 11.3°.

4.5 Shower leakage studies

As already mentioned, in this combined calorimeter test particles incident at an angle of 11.3° traverse about 11 interaction lengths, including passive materials at the back of the Tile calorimeter. Punchthrough particles can be muons from π and K decays in a hadronic cascade, or charged particles (mainly soft electrons and hadrons) and neutrons from showers not fully contained in the calorimeter. For this study, pions of 50, 100, 200 and 300 GeV were examined [9].

The probability of longitudinal shower leakage was defined as the fraction of events with a signal in at least one of the muon wall counters. To be considered as a punchthrough signal, the signal Q_i in any counter must satisfy the requirement

$$Q_i > (\overline{Q}_i^{\mu} - 3\sigma_i^{\mu}). \tag{8}$$

The average ($\overline{Q}_i^{\mu}$) and sigma values (σ_i^{μ}) were determined using the most probable energy deposition of muons in the muon wall.

Figure 14(a) shows the probability of longitudinal shower leakage as a function of the beam energy. The probability is corrected for the acceptance which is around 50% .At 100 GeV this probability is about 15%. The result is compared with the ones obtained by the RD5 [22] and CCFR [23] Collaborations for an iron equivalent thickness of 1.85 m as in the combined calorimeter setup. The measurements are in agreement with those of the CCFR Collaboration which used a very large detector for the punchthrough identification and therefore did not correct for the acceptance. The difference between the results of the RD5 and the CCFR Collaborations are discussed in Ref. [22]. The dashed line shows the expectation for the ATLAS configuration (10.6 λ at η = 0). Figure 14(b) shows the energy loss from leakage averaged over punchthrough events, defined as the difference between the mean energy values of events with and without a signal in the muon wall, for several beam energies. The energy loss for events with longitudinal leakage is about 3% at 100 GeV.

5 Summary and conclusions

A first test of the combined electromagnetic liquid argon and the hadronic Tile–iron calorimeter prototypes of the future ATLAS experiment was carried out, using pion beams of 20–300 GeV.

Two different methods of reconstructing the hadronic beam energy were used; the best resolution is obtained using a weighting technique, which gives $\sigma/E = ((46.5 \pm 6.0)\%/\sqrt{E} + (1.2 \pm 0.3)\%) \oplus (3.2 \pm 0.4)$ GeV$/E$.

The e/π ratio of the combined prototypes was found to be between 1.24 and 1.12, decreasing with energy as expected qualitatively from the variation with energy of the EM fraction of hadronic showers.

Energy resolutions, longitudinal profiles and e/π ratios are well reproduced by a simulation with standalone FLUKA, with some discrepancy for the lowest energy point.

The angular resolution in the θ direction for hadron showers was studied. The resolution can be described by the function $\sigma_\theta = (243.1 \pm 8.9)/\sqrt{E} + (12.1 \pm 0.7)$ mrad, which results in a σ_θ = 1.5° for a single hadron shower of 300 GeV.

Punchthrough studies show that even after about ten nuclear interaction lengths shower energy leakage at the highest energies is not negligible.

The results described in this paper show that the performance of the combination of these two calorimeters is close to the required specifications for hadron resolution [1]. However, in order to reconstruct the energy of jets, it will be necessary to measure the response of the combined calorimeters at lower incident hadron energies, down to a few hundred MeV. In addition,

more sophisticated energy reconstruction techniques will have to be developed to cope with overlapping signals from more than one hadron.

Acknowledgements

We sincerely thank the technical staffs of the collaborating Institutes for their important and timely contributions. Financial support is acknowledged from the funding agencies of the collaborating Institutes. Finally, we are grateful to the staff of the SPS, and in particular to K. Elsener, for the excellent beam conditions and assistance provided during our tests.

References

[1] ATLAS Technical Proposal, CERN/LHCC/94–43 LHCC/P2.

[2] D.M. Gingrich et al. (RD3 Collaboration), Nucl. Instr. and Meth. **A364** (1995) 290;
B. Aubert et al. (RD3 Collaboration), Nucl. Instr. and Meth. **A325** (1993) 118;
B. Aubert et al. (RD3 Collaboration), Nucl. Instr. and Meth. **A321** (1992) 467;
B. Aubert et al. (RD3 Collaboration), Nucl. Instr. and Meth. **A309** (1991) 438.

[3] F. Ariztizabal et al. (RD34 Collaboration), Nucl. Instr. and Meth. **A349** (1994) 384;
F. Ariztizabal et al. (RD34 Collaboration), LRDB Status Report, CERN/LHCC 95–44.

[4] O. Gildemeister, F. Nessi-Tedaldi and M. Nessi, *Proc. 2nd Int. Conf. on Calorimetry in High Energy Physics*, Capri, 1991.

[5] M. Bosman et al. (RD34 Collaboration), CERN/DRDC/93–3 (1993);
F. Ariztizabal et al. (RD34 Collaboration), CERN/DRDC/94–66 (1994).

[6] M. Cobal et al., ATLAS Internal Note, TILECAL-NO-067 (1995).

[7] D.E. Groom, Proc. of the *II International Conference on Calorimetry in High Energy Physics*, Capri 1991, (ed. A. Ereditato) World Scientific (1992) 376.

[8] T.A. Gabriel, D.E. Groom, P.K. Job, N.V. Mokhov and G.R. Stevenson, Nucl. Instr. and Meth. **A338** (1994) 336.

[9] M. Lokajicek et al., ATLAS Internal Note, TILECAL-NO-63 (1995);
M. Lokajicek et al., ATLAS Internal Note, TILECAL-NO-64 (1995).

[10] R. Wigmans, Nucl. Instr. and Meth. **A259** (1987) 389.

[11] W. Braunschweig et al. (H1 calorimeter group), report DESY 93–047;
D.M. Gingrich et al. (RD3 Collaboration), Nucl. Instr. and Meth. **A335** (1995) 295.

[12] R. Brun and F. Carminati, *GEANT Detector Description and Simulation Tool*, CERN Program Library, Long Writeup W5013, September 1993.

[13] C. Zeitnitz and T.A. Gabriel, *The GEANT–CALOR Interface User's Guide*, GCALOR version 1.04/07.

[14] A. Fassò, A. Ferrari, J. Ranft and P.R. Sala, Proc. of the workshop on *Simulating Accelerator Radiation Environment, SARE,* Santa Fè, 11-15 january (1993), A. Palounek ed., Los Alamos LA-12835-C (1994) 134;
A. Fassò, A. Ferrari, J. Ranft and P.R. Sala, Proc. of the *IV International Conference on Calorimetry in High Energy Physics*, La Biodola (Elba), September 19-25 1993, A. Menzione and A. Scribano eds., World Scientific (1994) 493;
A. Fassò, A. Ferrari, J. Ranft and P.R. Sala, Proc. of the 2nd workshop on *Simulating Accelerator Radiation Environment*, SARE-2, CERN-Geneva, October 9–11 1995, Yellow report CERN in press;
A. Ferrari and P.R. Sala, *The Physics of High Energy Reactions*, Proc. of the *Workshop on Nuclear Reaction Data and Nuclear Reactors Physics, Design and Safety*, International Centre for Theoretical Physics, Miramare-Trieste, Italy, 15 April–17 May 1996, World Scientific in press.

[15] A. Ferrari and P.R. Sala, ATLAS Internal Note, PHYS-NO-86 (1996).

[16] G. Battistoni, A. Ferrari and P.R. Sala, Proceedings of the *XXIV International Cosmic Ray Conference*, August 28-September 8 (1995), Roma, Italy, Vol 1, 597.

[17] P.R. Sala, talk given at the *VI Int. Conf. on Calorimetry in High Energy Physics*, Frascati (Rome), Italy, June 8–14 1996.

[18] K. Elsener, private communication.

[19] H.W. Atherton et al., CERN Yellow report CERN 80-07 (1980).

[20] I. Efthymiopoulos, talk given at the *VI Int. Conf. on Calorimetry in High Energy Physics*, Frascati (Rome), Italy, June 8–14 1996,.

[21] H. Plothow-Besch, ATLAS Internal Note, TILECAL-NO-70 (1995).

[22] M. Aalste et al. (RD5 Collaboration), Z. Phys. **C60** (1993) 1;
M. Aalste et al. (RD5 Collaboration), CERN-PPE/95-61

[23] F.S. Merrit et al. (CCFR Collaboration), Nucl. Instr. and Meth. **A245** (1986) 27.

Table 1: Mean energy, σ and fractional energy resolution for the various beam energies using the 'benchmark' approach.

Energy	E_{rec} (GeV)	σ_{rec} (GeV)	$\frac{\sigma_{rec}}{E_{rec}}(\%)$
20 GeV	20.1 ± 0.2	4.1 ± 0.1	20.6 ± 0.7
50 GeV	49.9 ± 0.4	5.7 ± 0.1	11.4 ± 0.3
100 GeV	100.7 ± 0.7	7.7 ± 0.2	7.7 ± 0.2
150 GeV	150.3 ± 1.3	9.6 ± 0.7	6.4 ± 0.5
200 GeV	202.6 ± 1.5	11.5 ± 0.2	5.6 ± 0.1
300 GeV	298.7 ± 2.2	14.8 ± 0.2	4.94 ± 0.07

Table 2: Mean energy, σ and fractional energy resolution for the various beam energies using the 'weighting' technique.

Energy	E_{rec}^{corr} (GeV)	σ_{rec}^{corr} (GeV)	$\frac{\sigma_{rec}^{corr}}{E_{rec}^{corr}}(\%)$
20 GeV	19.9 ± 0.7	3.9 ± 0.2	19.8 ± 1.2
50 GeV	51.2 ± 0.3	5.3 ± 0.1	10.3 ± 0.3
100 GeV	102.5 ± 0.6	6.8 ± 0.1	6.6 ± 0.1
150 GeV	152.2 ± 1.2	8.7 ± 0.9	5.7 ± 0.6
200 GeV	204.5 ± 1.3	10.2 ± 0.1	4.99 ± 0.08
300 GeV	296.9 ± 2.0	12.0 ± 0.2	4.03 ± 0.06

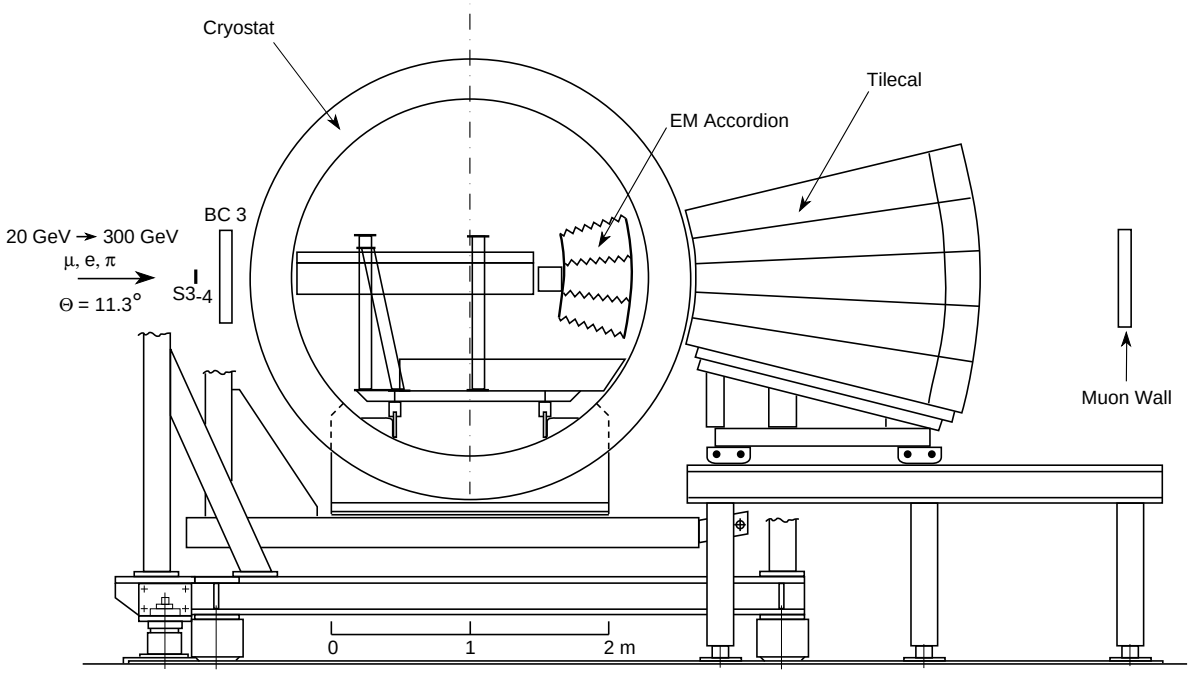

Figure 1: Test beam setup for the combined LAr and Tile calorimeter run.

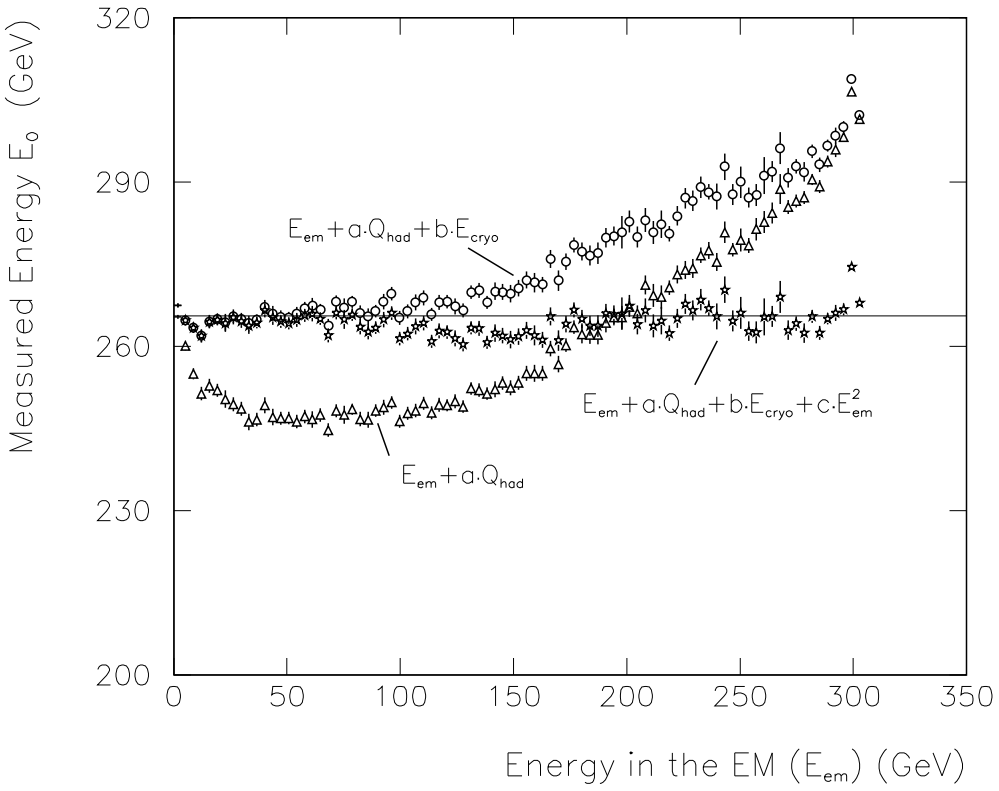

Figure 2: Components of the first pass energy E_0 vs. energy in the EM calorimeter using the 'benchmark' energy reconstruction method for 300 GeV pions.

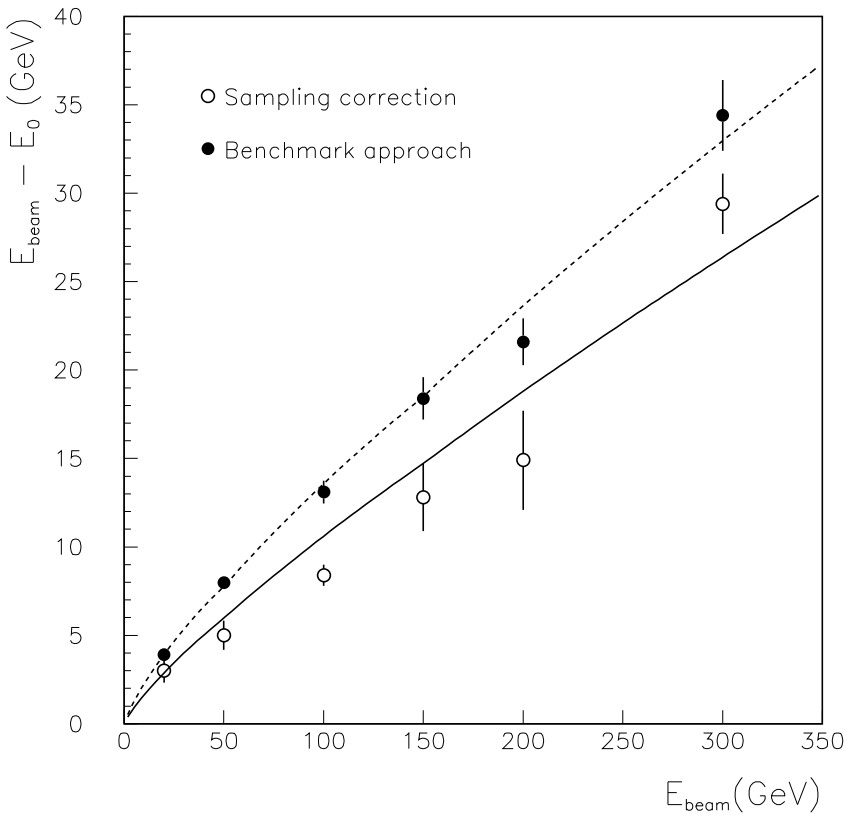

Figure 3: Difference between the beam energy and the first pass hadron energy E_0 as a function of the beam energy. The black points are obtained with the benchmark method, the empty circles with the weighting method. Fits of the form given in eq. 2 to the two sets of points are shown.

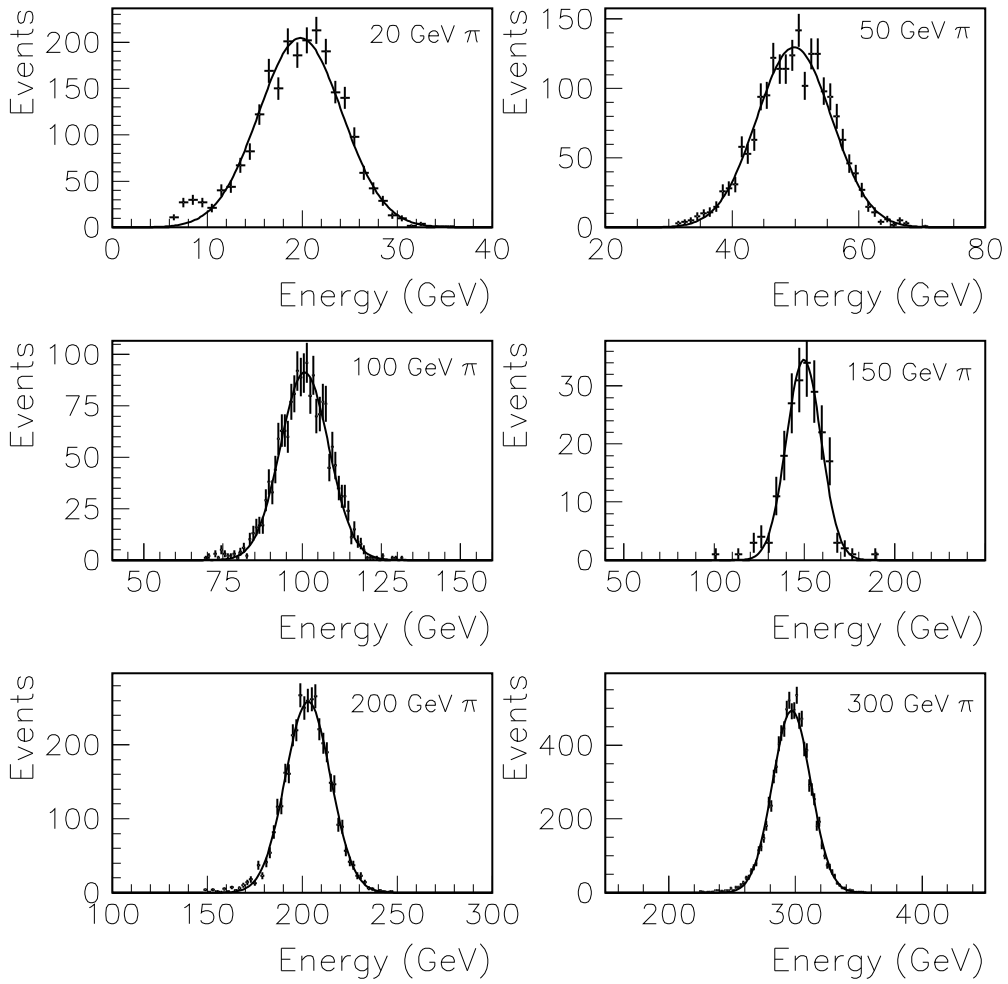

Figure 4: Pion energy spectra at different incident energies, obtained with the benchmark algorithm. The mean and σ values are listed in Table 1.

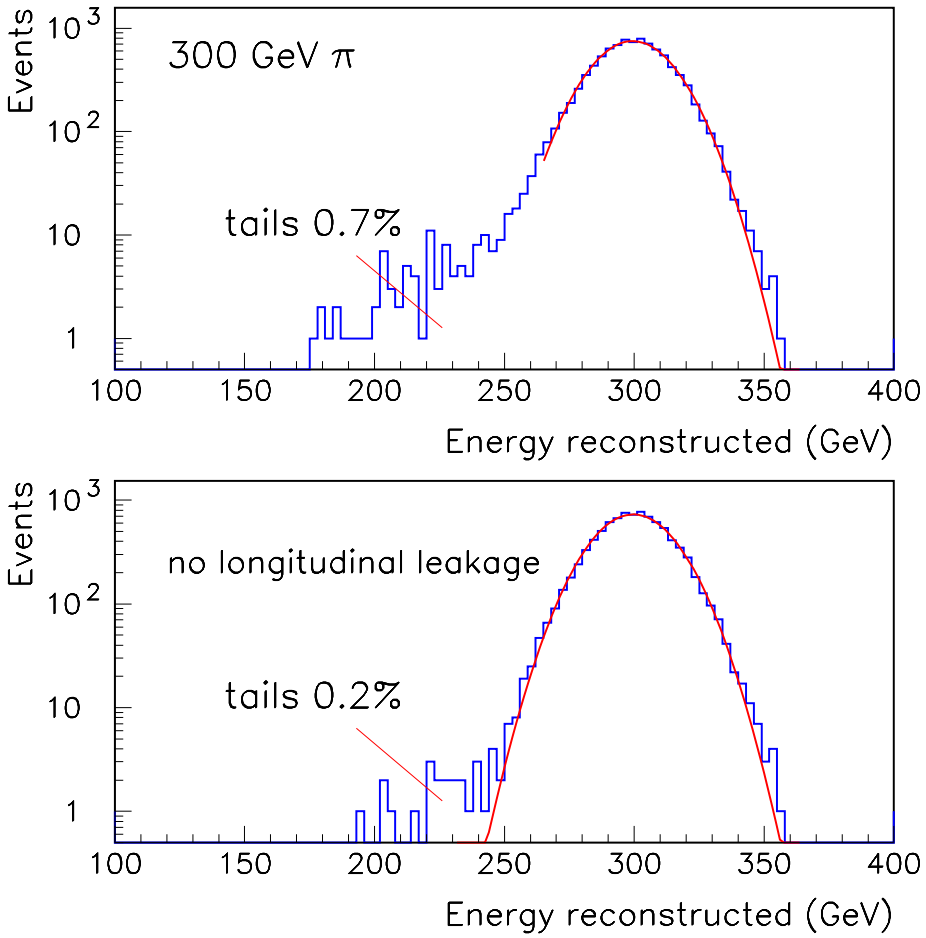

Figure 5: Low energy tails in the 300 GeV pion spectrum before (upper plot) and after (lower plot) rejecting the events with a signal in the muon wall.

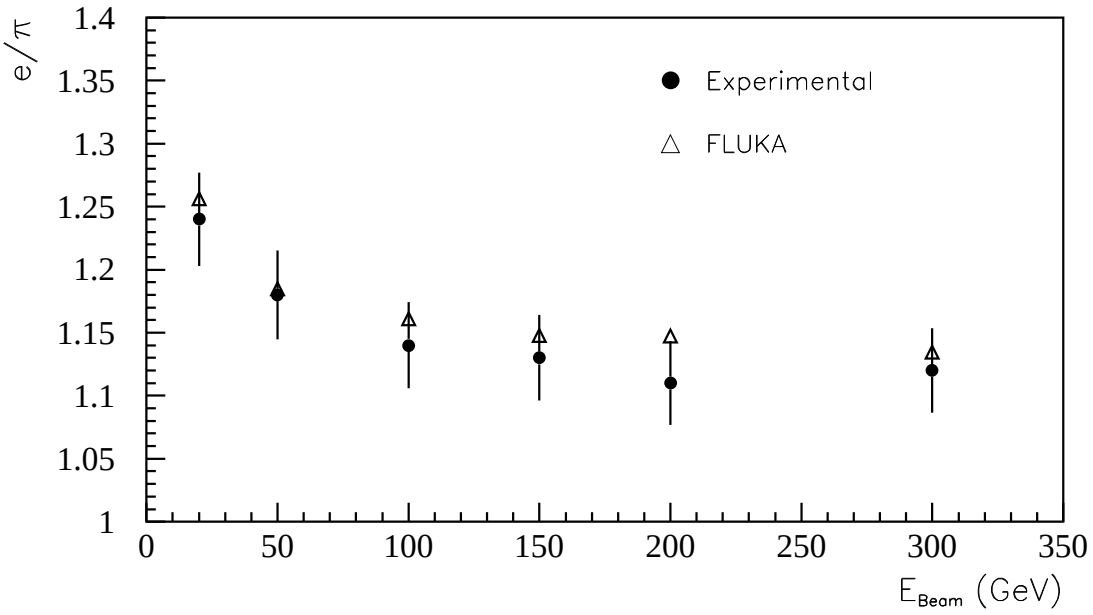

Figure 6: Values of the e/π ratio vs. the beam energy. Standalone FLUKA results are also shown.

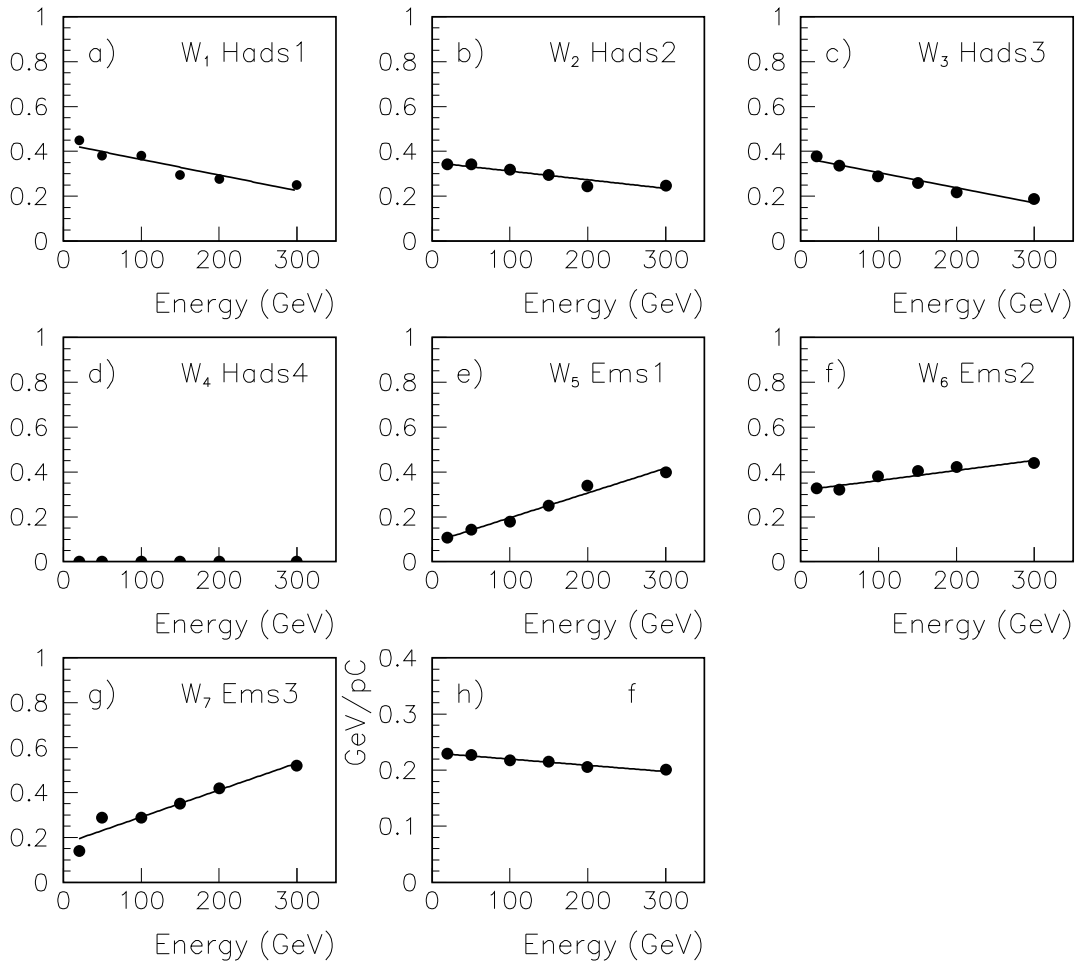

Figure 7: Parametrization of the weight for each longitudinal sampling and of the intercalibration parameter as a function of the beam energy.

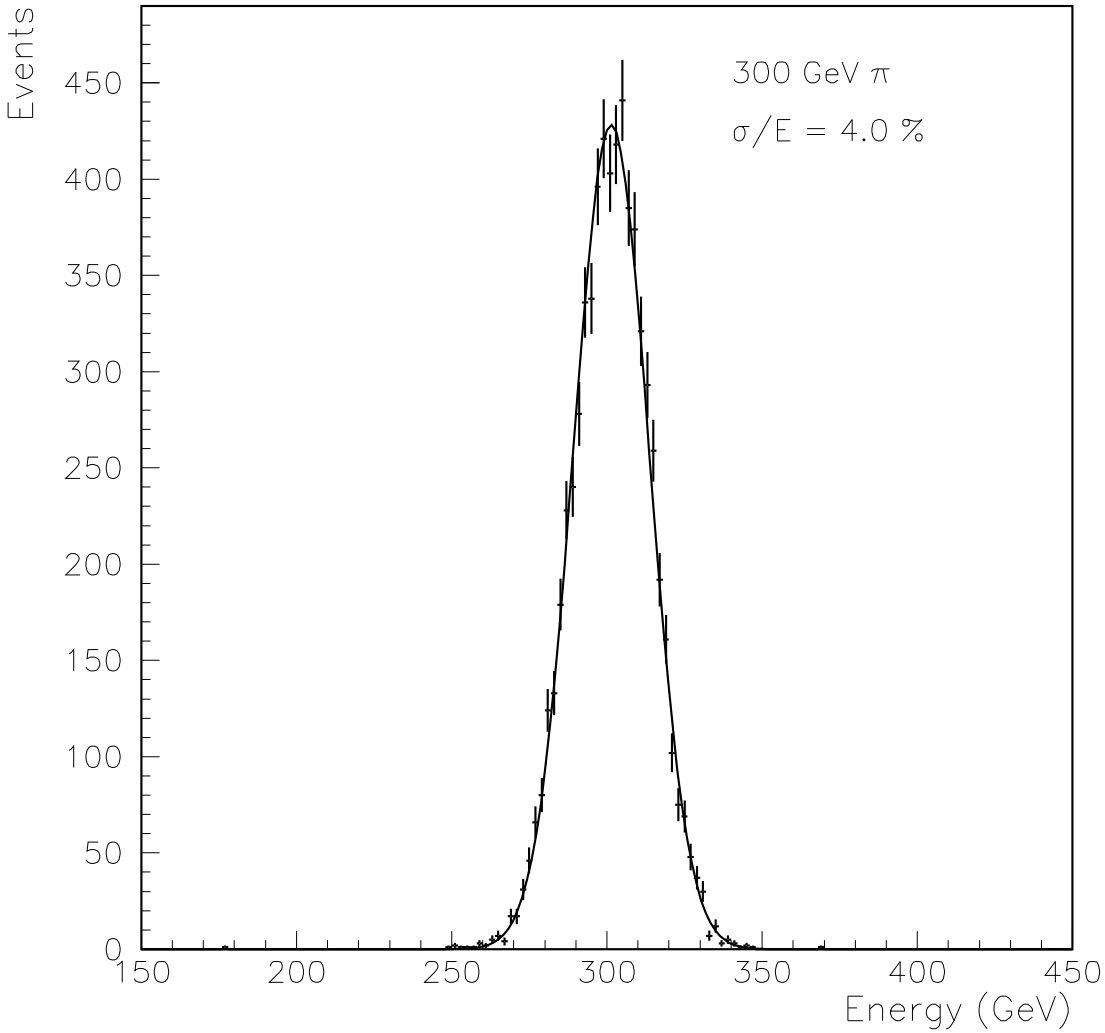

Figure 8: Energy spectrum of 300 GeV pions, where the energy is reconstructed with the weighting method.

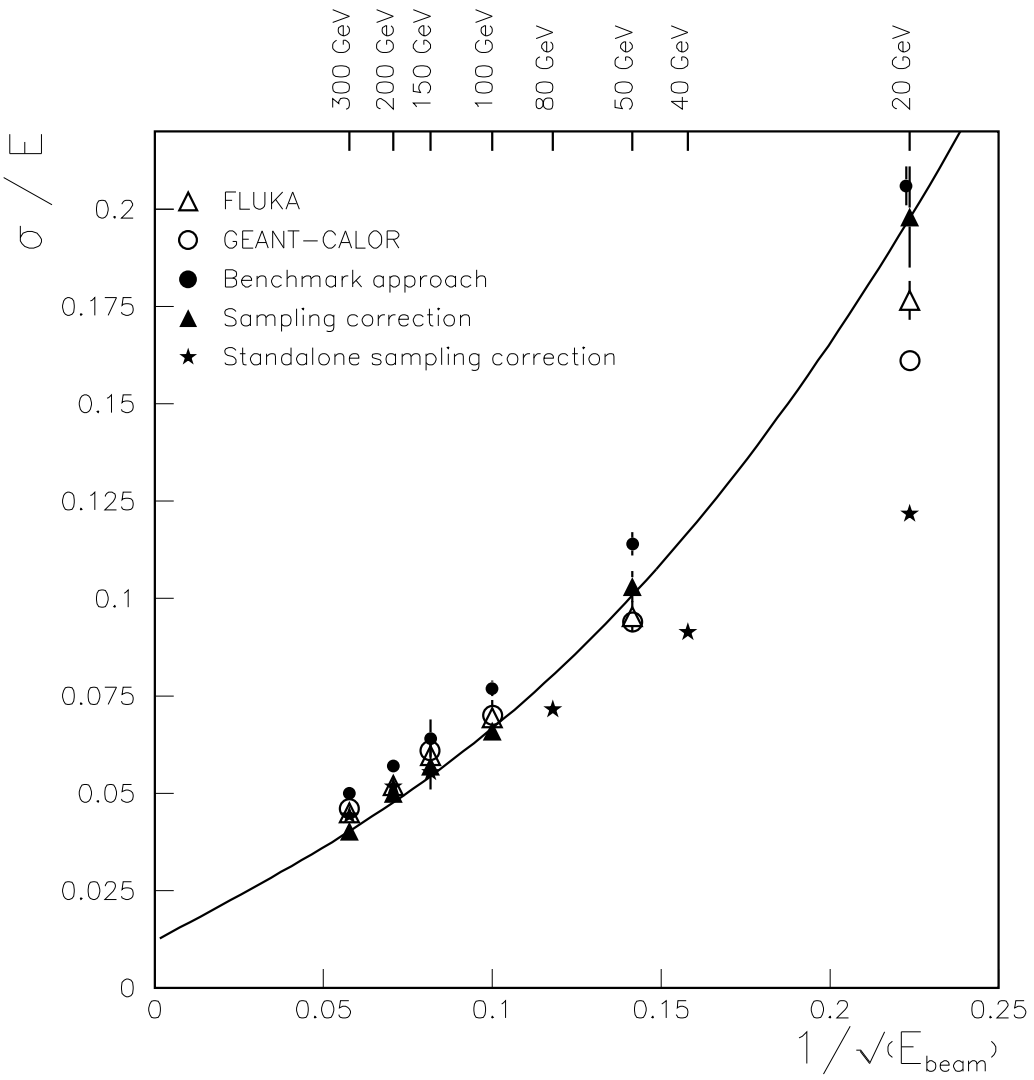

Figure 9: Energy resolutions with the benchmark approach and with the weighting method ('sampling corrections'). The data are compared with the combined Monte Carlo simulations and with the results from the stand-alone hadron calorimeter test beam (stars).

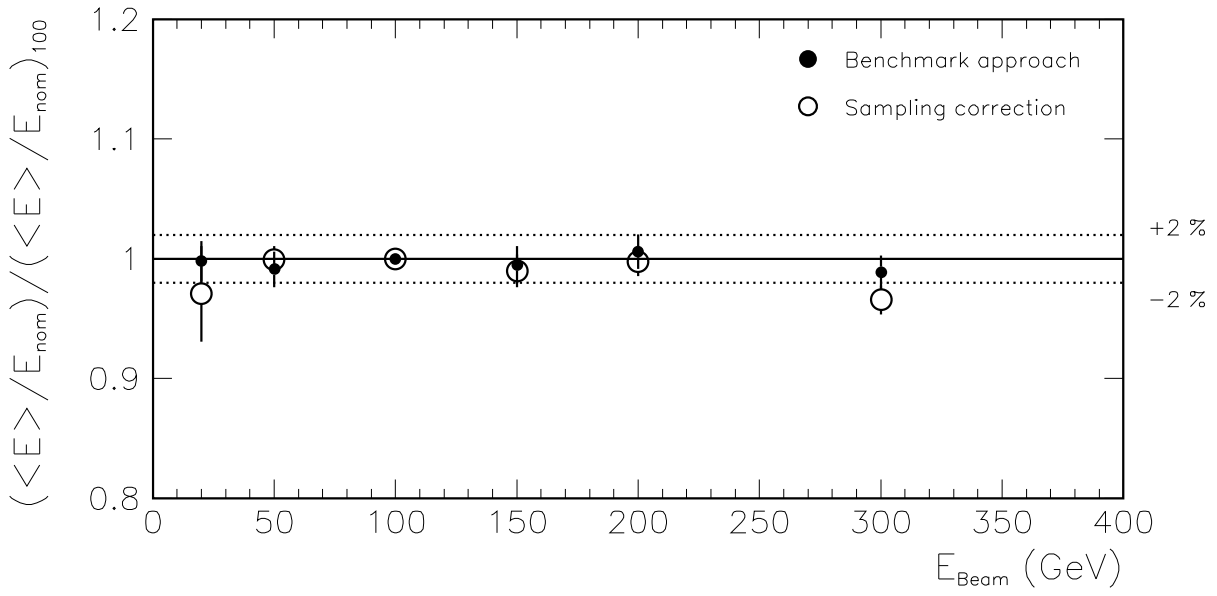

Figure 10: Linearity of the pion response with the benchmark approach and with the weighting method (‘sampling corrections’). All the points are normalized to the point at 100 GeV.

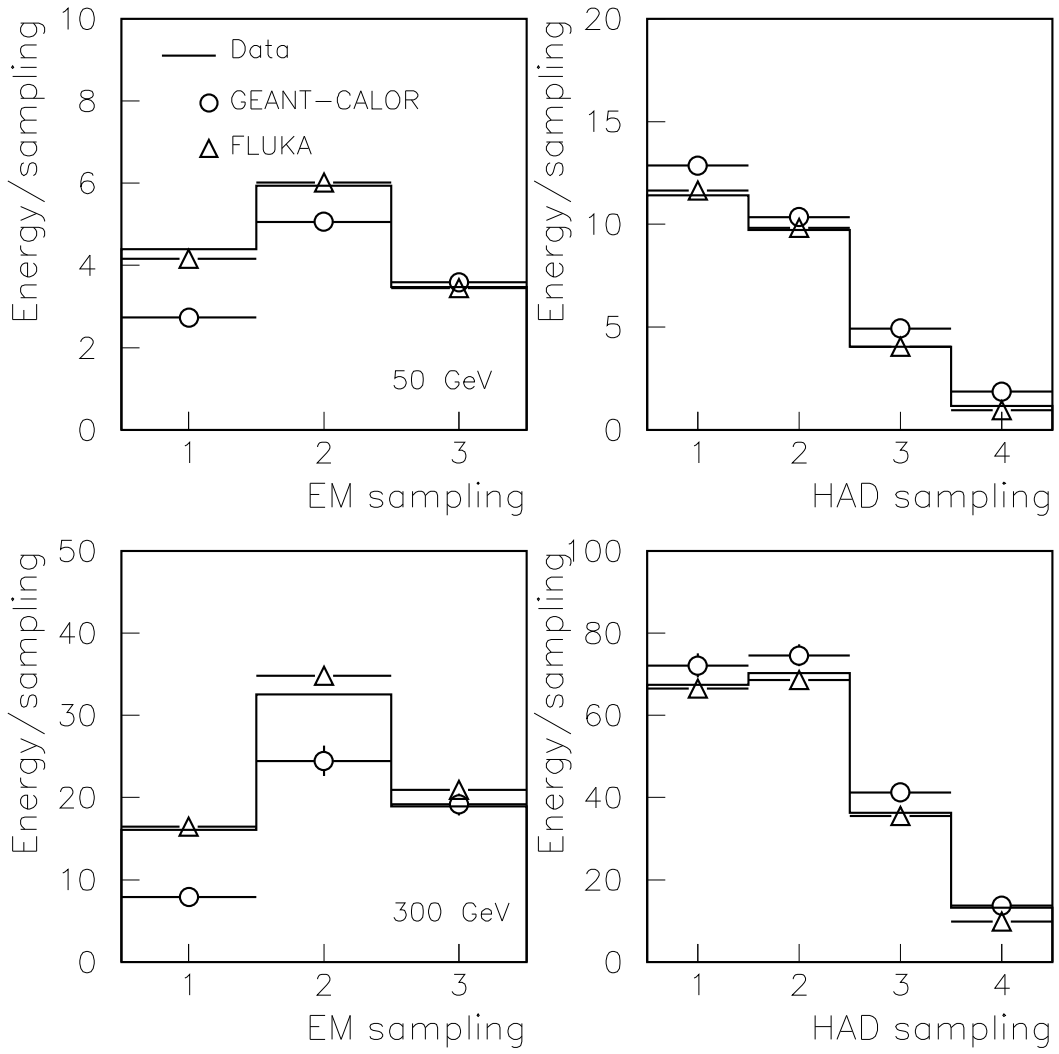

Figure 11: Energy deposition in each sampling of the electromagnetic (on the left) and hadronic (on the right) calorimeters for pions of 50 (on top) and 300 GeV (on bottom). The data are compared with both Monte Carlo simulations.

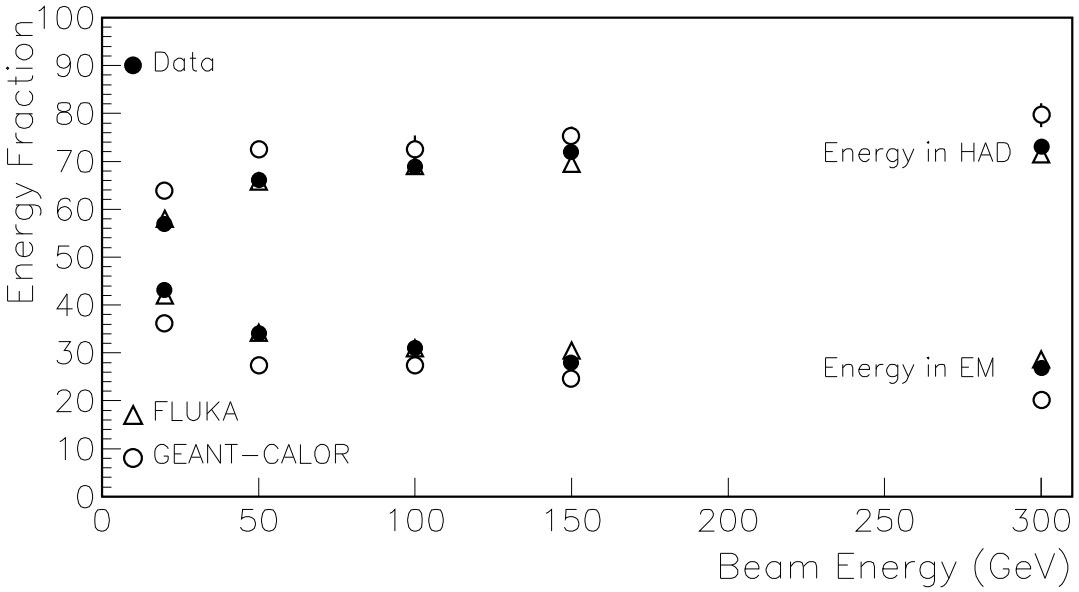

Figure 12: Energy deposition (percentage) in the electromagnetic and hadronic calorimeters for the data and the Monte Carlo simulations, at different beam energies.

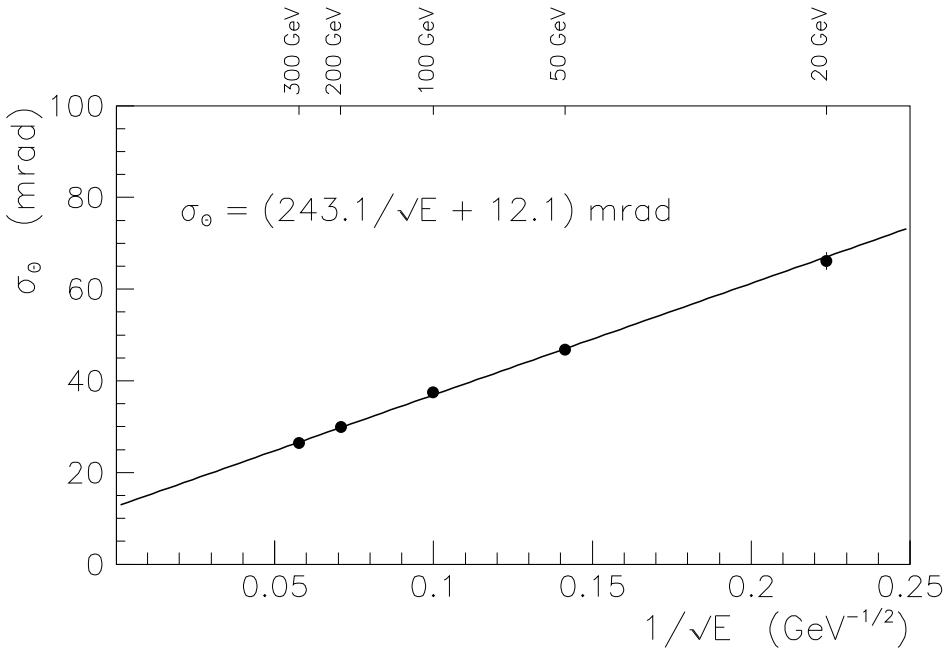

Figure 13: Angular resolution for pions as a function of the beam energy.

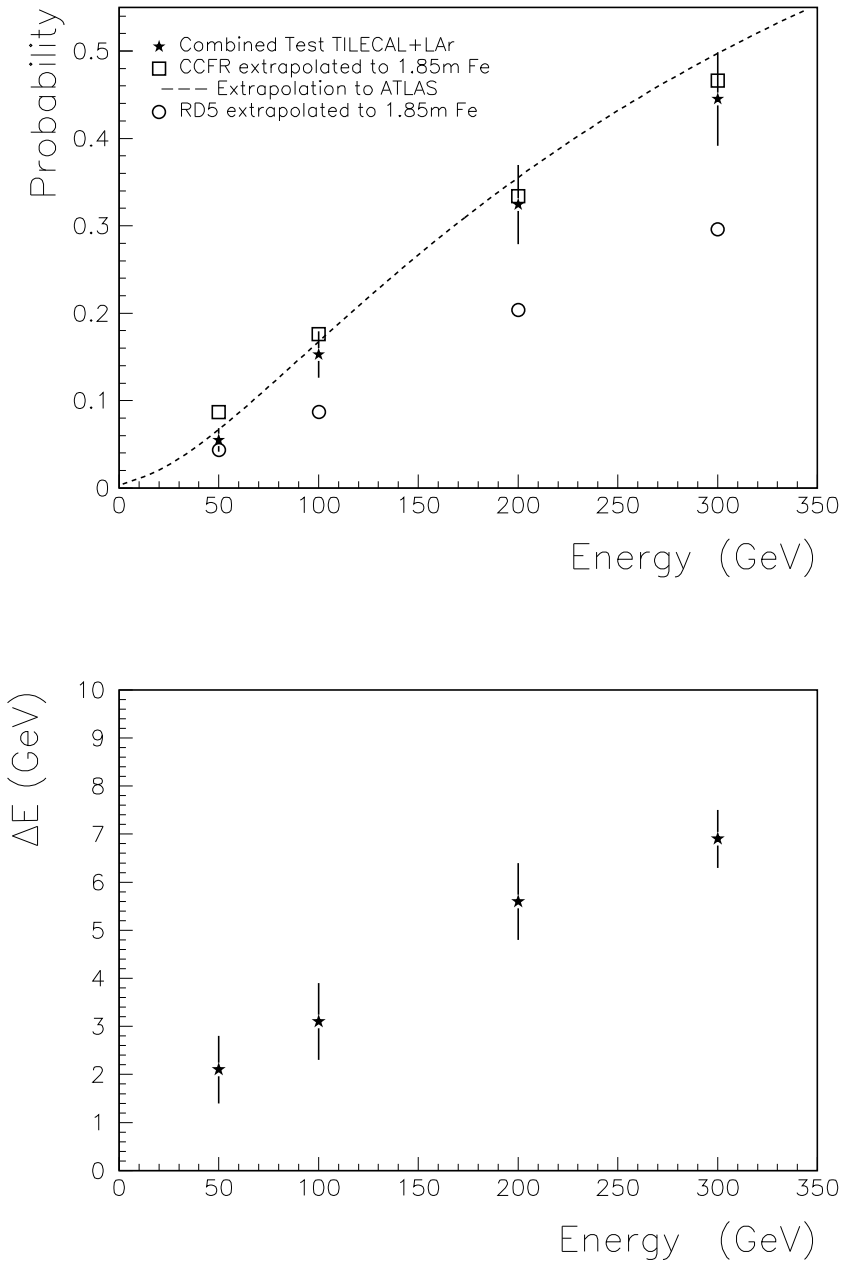

Figure 14: (a) Punchthrough probability for pions. Results from the RD5 and CCFR Collaboration (recalculated for 1.85 m of iron) are also plotted. The dashed line shows the expectation for the ATLAS configuration. (b) Average energy loss vs. beam energy for events with longitudinal leakage.